scientific reports

Check for updates

OPEN

Effective degradation of Reactive Blue 21 and Reactive Red 195 by copper(II) oxide nanoparticles biosynthesized by pistachio hulls extract

Seyed Mohammad Sadegh Hosseini✉, Mohammad Ali Maghool & Hadis Eghbali

Textile dyes such as Reactive Blue 21 and Reactive Red 195 are complex organic compounds widely used in the fabric industry, which often cause significant environmental pollution due to their resistance to conventional wastewater treatment methods. The aim of this study is photo-degradation of these organic dyes by copper (II) oxide nanoparticles (CuO-NPs) that biosynthesized via a method based on pistachio hulls extract. The synthesized nanoparticles were characterized by various techniques such as X-ray diffraction (XRD), scanning electron microscopy (SEM), Fourier-transform infrared spectroscopy (FT-IR), dynamic light scattering (DLS), and ultraviolet-visible (UV-Vis) spectroscopy. The characterization results confirm the formation of homogeneous, spherical, crystalline CuO-NPs with an average size of approximately 90 nm. The high quality of CuO-NPs synthesized using pistachio hull extract is attributed to the presence of natural reducing and capping agents in the extract. These agents play a dual role: they reduce the copper precursor to CuO-NPs and simultaneously stabilize the nanoparticles by preventing agglomeration. The biosynthesized CuO-NPs showed high photocatalytic activity in degrading organic dyes under UV light irradiation. Specifically, the degradation efficiencies reached about 83% for Reactive Blue 21 and 75% for Reactive Red 195 after 180 min of irradiation.

Keywords Pistachio hull extract, Biosynthesis, CuO-NPs, Degradation, Reactive Red 195

Textile dyes represent a significant class of environmental pollutants, posing a severe threat to aquatic ecosystems and human health. A substantial volume of these synthetic, complex organic compounds is discharged in the effluent from textile industries, leading to the contamination of water bodies. This not only causes aesthetic pollution but also drastically reduces light penetration and dissolved oxygen, disrupting photosynthesis and aquatic life. Furthermore, many dyes and their breakdown products are toxic, mutagenic, and carcinogenic, accumulating in the food chain. Their complex aromatic molecular structures render them stable and resistant to conventional degradation processes[1,2]. Therefore, the development and implementation of effective treatment technologies for the complete degradation and removal of these hazardous dyes are of paramount importance to safeguard water resources, protect biodiversity, and ensure public health[3,4].

Reactive Blue 21 (Fig. 1a) with is characterized by a large, planar anthraquinone backbone, which gives it its intense blue color and stability. Reactive Blue 21 exhibits highly soluble in water due to its sulfonic acid groups. Primarily used for dyeing cellulose fibers like cotton, viscose, and linen. It forms a covalent bond with the fiber in an alkaline medium. The anthraquinone structure makes it highly stable against light, washing, and oxidizing agents. This very stability is what makes it persistent in the environment. While generally considered to have low acute toxicity, its breakdown products may be harmful. Its persistence in water is a major concern. When released in wastewater, it reduces light penetration in water bodies, severely affecting photosynthesis and aquatic life. Its complex structure resists biodegradation in conventional treatment plants[5].

The molecular structure of Reactive Red 195 (Fig. 1b) contains the characteristic azo group (-N = N) bridging aromatic rings. This group is the chromophore responsible for its red color. Like Reactive Blue 21, it is used for dyeing cellulose fibers. It reacts with the fiber through its reactive groups under alkaline conditions. Azo dyes

Chemical Engineering Department, Vali-e-Asr University of Rafsanjan, Rafsanjan, Iran. ✉email: chehosseini@gmail.com

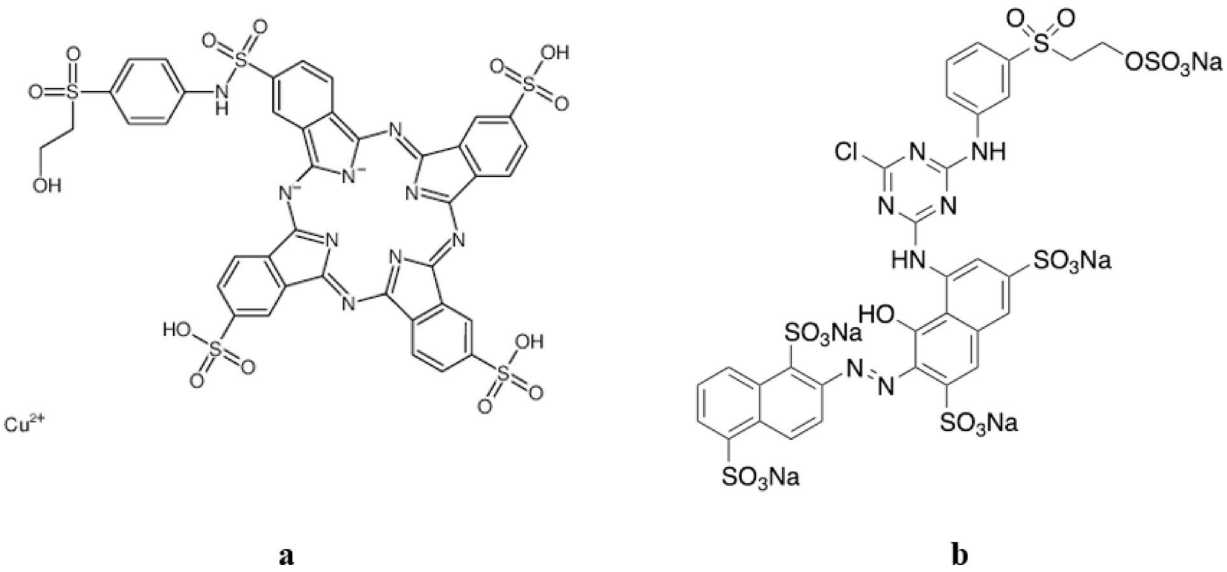

Fig. 1. Molecular structure of (**a**) Reactive Blue 21, (**b**) Reactive Red 195[6].

are generally stable, but the azo bond (-N = N-) can be cleaved under certain conditions, which is a key pathway for its degradation. The primary concern with azo dyes like RR195 is that under anaerobic conditions, they can break down to produce aromatic amines, many of which are known to be carcinogenic and mutagenic. It contributes to the color pollution of water and poses a potential toxic threat to aquatic organisms and humans due to the possible formation of harmful breakdown products[5].

The removal of organic dyes from wastewater is a critical environmental challenge. Two prominent and often complementary methods for this are adsorption and photocatalytic degradation. Adsorption is a physical surface process where dye molecules (adsorbate) accumulate on the surface of a solid material (adsorbent). Dye molecules are attracted and bound to the adsorbent's surface through various forces, including: Physical Adsorption (Weak Van der Waals forces (, Chemical Adsorption (Stronger covalent or ionic bonding), and Electrostatic Interaction (Attraction between oppositely charged dye ions and the adsorbent surface)[7]. Adsorption is a transfer process, not a destruction process. It concentrates the pollutants onto the solid adsorbent, creating a secondary waste (spent adsorbent) that requires further treatment or disposal. On the other hand, it is not effective for high concentrations of dye. Photocatalysis is an advanced oxidation process that destroys dye molecules, converting them into harmless end products like CO_2, H_2O, and mineral acids. The process is driven by a semiconductor photocatalyst (e.g., TiO_2, ZnO, CuO) upon light irradiation. When the photocatalyst absorbs photons with energy equal to or greater than its bandgap energy, electrons (e^-) are excited from the valence band (VB) to the conduction band (CB), creating positive holes (h^+) in the VB. The electron-hole pairs migrate to the catalyst's surface. The positive hole (h^+) reacts with water (H_2O) or hydroxide ions (OH^-) to generate highly reactive hydroxyl radicals (•OH). These powerful reactive oxygen species, especially the •OH radical, non-selectively attack and oxidize the complex organic dye molecules, breaking them down into smaller, non-toxic intermediates and ultimately mineralizing them[8]. The primary advantage is the complete destruction and mineralization of pollutants, eliminating the disposal problem associated with adsorption. In an ideal wastewater treatment system, adsorption and photocatalysis work synergistically[9]. The photocatalyst first adsorbs the dye molecules onto its large surface area. This concentrates the pollutants near the site of reaction. Upon light irradiation, the photocatalytic degradation process is initiated, destroying the adsorbed dye molecules. As the dye is degraded, the adsorption sites on the photocatalyst are regenerated, allowing the process to continue efficiently[9].

Research on the photocatalytic degradation of Reactive Red 195 is indeed scarce compared to Reactive Blue 21. Most studies focus on similar dyes or other related reactive azo dyes, but direct investigations into Reactive Red 195 are limited. This scarcity may be due to the dye's structural complexity. The paper by Rodrigues et al. presents a comprehensive study of ZnO nanoparticles as photocatalysts for degrading Reactive Blue 21 dye in aqueous solution. According to Rodrigues study, ZnO nanoparticles efficiently photodegrade Reactive Blue 21 dye through a photocatalytic process aided by optimized catalyst loading and particle size. The integrated experimental and modeling approach offers insight for scaling and optimizing photocatalytic wastewater treatment using ZnO nanoparticles[10]. El-Bindary et al. investigated photocatalytic degradation mechanisms of Reactive Blue 21 over Ag/ZnO nanoparticles using scavengers to identify reactive species. Based on their study, silver-doped zinc oxide (Ag-ZnO) nanoparticles have shown enhanced photocatalytic degradation performance for Reactive Blue 21 dye compared to pure ZnO nanoparticles. Ag doping improves photocatalytic efficiency mostly by reducing electron-hole recombination, which increases the generation of reactive species that degrade dye molecules. They reported degradation efficiency of Reactive Blue 21 using Ag-ZnO photocatalysts reaches above 90% within about 90 min under UV or visible light irradiation. The photocatalytic activity remains stable over multiple cycles with minimal activity loss due to catalyst recovery losses[11].

Materials	Chemical formula	Company
Copper(II) sulfate pentahydrate	$CuSO_4.5H_2O$	Merck
Ethanol	C_2H_5OH	Merck
Reactive Blue 21	$C_{40}H_{25}CuN_9O_{14}S_5$	Sys-Arang
Reactive Red 195	$C_{31}H_{19}ClN_7Na_5O_{19}S_6$	Sys-Arang
Pistachio hulls	----	Sourced from one of the pistachio orchards in Rafsanjan Region (Akbari variety)

Table 1. The list of various chemicals, precursor and solvent used in this study.

Fig. 2. Fresh (**a**), and air-dried pistachio hulls (**b**).

Sarkar et al. employed titanate nanotubes (TNTs) for adsorption and photo-degradation of Reactive Blue 21, demonstrating effective removal under UV light. Photo-degradation experiments under UV light and adequate oxygen availability showed that TNTs efficiently catalyze the degradation of Reactive Blue 21. A proposed photo-degradation mechanism involves generation of reactive oxygen species at the TNT surface under UV excitation, which oxidizes the dye molecules[12].

The study by Jouali et al. investigated the performance of TiO_2-cellulose composites as robust, recyclable photocatalysts for wastewater treatment. This study showed that TiO_2 particles immobilized on cellulosic fibers can effectively and sustainably degrade organic dyes like methylene blue and Reactive Blue 21 under dynamic flow, merging photocatalytic degradation with adsorption benefits while ensuring catalyst recyclability[13]. The study by Atrak, et al. focuses on the green synthesis of $Zn0.5Ni0.5AlFeO_4$ magnetic nanoparticles using tragacanth gel via a sol-gel method. These nanoparticles were characterized thoroughly by FTIR, XRD, FESEM, EDX, and VSM techniques, confirming a single-phase cubic spinel structure with an average crystallite size around 10 nm and good magnetic properties (saturation magnetization 33.82 emu/g). The photocatalytic activity of these magnetic nanoparticles was investigated for the degradation of Reactive Blue 21 dye under visible light irradiation. The study examined effects of photocatalyst dosage, initial dye concentration, pH, and contact time on the degradation efficiency. The $Zn0.5Ni0.5AlFeO_4$ nanoparticles exhibited high photocatalytic activity, achieving up to 94% degradation of Reactive Blue 21[14].

In most photocatalytic works, semiconductor nanostructures such as titanium oxide (TiO_2), zinc oxide (ZnO), and copper oxide (CuO) are commonly synthesized using physicochemical methods like co-precipitation, sol-gel, and hydrothermal techniques. These methods are popular due to their ability to produce nanoparticles with controlled size, morphology, and crystallinity, which enhances photocatalytic activity. Modifications such as doping, heterojunction formation, and surface functionalization are often combined with these synthesis methods to enhance visible-light absorption and reduce charge recombination[15]. These synthesis methods are usually associated with high energy consumption, and the employment of toxic reducing and stabilizing agents. These conditions not only increase environmental costs but can also have significant negative effects on the health of living organisms[16].

In green or bio synthesis of metal and metal oxide nanoparticles, various biological systems such as bacteria, fungi, algae, and different parts of plants including flowers, roots, leaves, and fruits are used. Among these options, plant extracts have attracted the most attention due to their abundance, low cost, biocompatibility, and the simplicity of the process, especially for large-scale nanoparticle synthesis. This method is often slow but highly efficient and environmentally friendly. Plant extracts contain various compounds like ketones, aldehydes, flavonoids, amides, terpenoids, carboxylic acids, phenols, and ascorbic acid. These compounds can act as reducing and stabilizing agents, converting metal ions into stable nanoparticles. The green synthesis process depends on several factors such as the type of precursor, solvent conditions, temperature, pressure, and pH. The

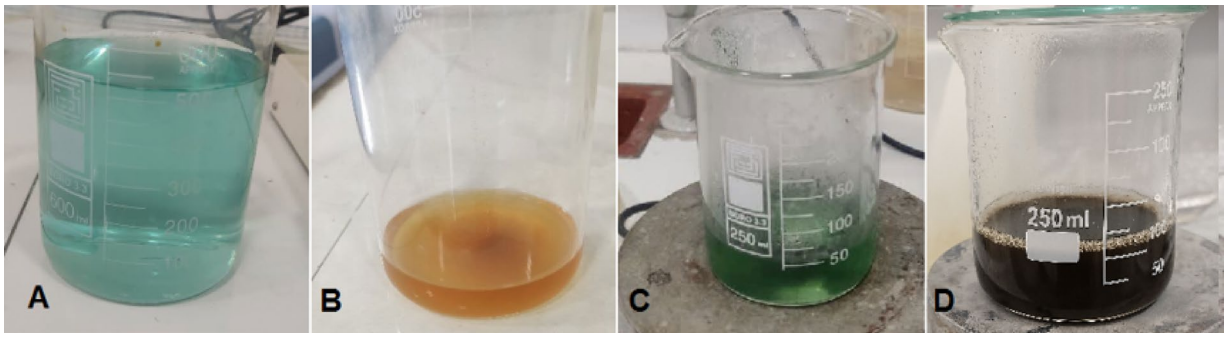

Fig. 3. Biosynthesis of copper oxide nanoparticles: (**A**) copper sulfate solution (**B**) pistachio hull extract (**C**) copper sulfate solution during addition of extract (**D**) formation of CuO nanoparticles.

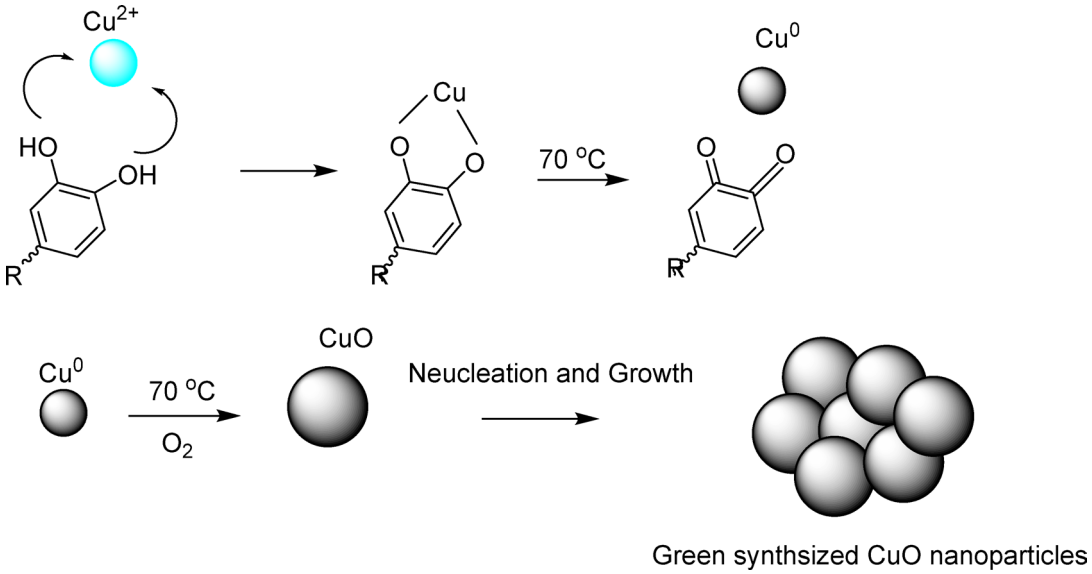

Fig. 4. Schematic representation of biosynthesis mechanism of CuO-NPs.

biodiversity of plants, their availability, and richness in bioactive compounds make them a suitable source for reducing metal salts and producing nanoparticles[17–20].

Recent literature reviews confirm a marked surge in research on the biosynthesis (green synthesis) of CuO nanoparticles. For example, CuO nanoparticles were synthesized using Euphorbia heterophylla leaf extract[21], Hagenia abyssinica extract[22], Juglans regia[23], Cocculus hirsutus[24], Catha edulis extract[25], Eichhornia crassipes[26], Justicia gendarussa[27], Psidium guajava[28], Citrofortunella microcarpa[29], Portulaca oleracea[30], Falcaria vulgaris[31], Solanum melongena[32]. Black barberry (Berberis integerrima)[33], Cistus creticus[34], Laurus nobilis[35], Eucalyptus globulus[36], Stachys lavandulifolia[37], Solanum nigrum[38], Solanum lycopersicum[39], Crocus sativus (saffron)[40], Moringa oleifera[41].

The pistachio hull is the soft, fleshy, and often reddish outer covering that surrounds the hard, beige shell of the pistachio nut. During the processing and dehulling of pistachios, this outer layer is removed as a primary by-product. Rafsanjan, located in Kerman Province, is the heart of pistachio production in Iran. Iran is one of the world's largest producers and exporters of pistachios, making Rafsanjan a globally significant region for this crop. It is estimated that for every ton of fresh pistachio nuts harvested, approximately a few hundred kilograms of wet hulls are produced. Given the massive scale of pistachio cultivation in the Rafsanjan area, this results in the generation of a very large and abundant agricultural waste stream each year. The concentration of the harvest and processing season means that a huge quantity of hulls is generated in a short period. This creates a significant waste management challenge for local farmers and processing units, as the fresh hulls are prone to rapid decomposition and can cause environmental issues if not managed properly. Pistachio hulls are not just waste; they are a source of valuable plant compounds which candidate it for green synthesis of metal and metal oxide nanoparticles. While pistachio hull composition may vary seasonally, the Akbari variety used here is cultivated under standardized agronomic practices in Rafsanjan Large-scale extract standardization (e.g., total phenolic content) would be implemented industrially to ensure reproducibility.

The principal aim of this study is to synthesize copper oxide nanoparticles through an environmentally benign, bio synthesis route utilizing an aqueous extract of pistachio hulls as a reducing and stabilizing agent. The biosynthesized CuO-NPs were comprehensively characterized and subsequently applied as a heterogeneous photocatalyst for the degradation of two model organic pollutants: Reactive Blue 21 and Reactive Red 195. The photocatalytic performance was systematically evaluated first for individual dye solutions and then for a binary dye mixture to investigate the competitive kinetics and interaction effects between the two dyes under simulated light irradiation. This work highlights a sustainable approach for both nanomaterial synthesis and wastewater treatment, addressing the challenge of complex dye effluents.

Experimental

Materials

The materials for the extraction and the synthesis of CuO-NPs, as well as for the investigation of dye degradation are listed in Table 1.

Methods

Extraction

First, fresh pistachio hulls (Akbari variety) were collected from orchards in the vicinity of Rafsanjan. The hulls were washed with distilled water to remove dust and contaminants. Then, they placed in the shade and exposed to fresh air for two weeks to dry slowly. After complete drying, the dried-hulls were finely ground with an electric mill to prepare them for extraction. 5 gr of ground pistachio hull were added to 100 mL of distilled water. The mixture was then placed on a shaker at 40 °C and stirred for 24 h. After this period, the extract suspension was first passed through a clean filter to remove the coarse particles. The solution was then centrifuged 20 min at 3000 rpm to separate the fine solid particles. After centrifugation, the solution was transferred to a refrigerator at 4 °C for subsequent steps (Fig. 2).

Biosynthesis of CuO-NPs

Initially, the copper sulfate solution (0.01 M) was placed on a hotplate stirrer and heated to approximately 70 °C. The pistachio hull extract (30 mL) was then added slowly and dropwise to the solution over 180 min under continuous stirring. The initial pH of the reaction mixture was acidic, measured at around 4, and no external adjustment was applied during synthesis. During this process, the color of the solution gradually changed from blue to dark green and finally to dark brown, which is a well-established visual indicator of CuO nanoparticle formation. This progressive color transition reflects the reduction of Cu^{2+} ions and the nucleation of CuO nanoparticles, confirming successful biosynthesis under controlled acidic conditions (Fig. 3).

Phenolic compounds in pistachio hull extract, such as gallic acid and rutin, are known to have antioxidant properties and can act as both reducing and stabilizing agents in nanoparticle synthesis. These phenols can complex with copper ions (Cu^{2+}), binding to them through their functional groups (mechanism described in Fig. 4). Through this complexation, the phenols facilitate the reduction of Cu^{2+} ions to copper (Cu^0) or copper oxide nanoparticles (CuO), effectively serving as natural reducing agents[37]. This process also stabilizes the nanoparticles formed, preventing agglomeration. The antioxidant properties of these phenolic compounds are key to this green synthesis, enabling a simple, eco-friendly method to produce Cu or CuO nanoparticles using pistachio hull extract without toxic chemicals[42]. The reduction of Cu^{2+} ions in the presence of pistachio hull extract can be attributed to the electron-donating ability of phenolic acids and flavonoids. Hydroxyl (-OH) and carbonyl (C = O) groups in these compounds chelate copper ions, forming intermediate complexes that undergo reduction to CuO nuclei under mild heating. Simultaneously, these phytochemicals adsorb onto the nanoparticle surface, acting as stabilizers and preventing particle aggregation.

After cooling, the final solution was centrifuged at 7000 rpm about 3 min. Subsequently, the obtained solid was washed with ethanol and centrifuged three times and finally transferred to an oven for drying (80 °C,12 h). Then, the dried solid was moved to a furnace for calcination at 300 °C for 5 h. This obtained solid was used for characterization and photocatalytic applications. To identify and characterize biosynthesized CuO-NPs,

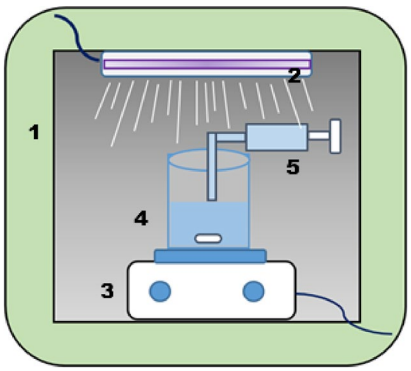

Fig. 5. Schematic representation of the wooden chamber equipped with UV lamp. (1: wooden chamber, 2: UV lamp, 3: magnetic stirrer, 4: batch reactor, 5: sampling syringe).

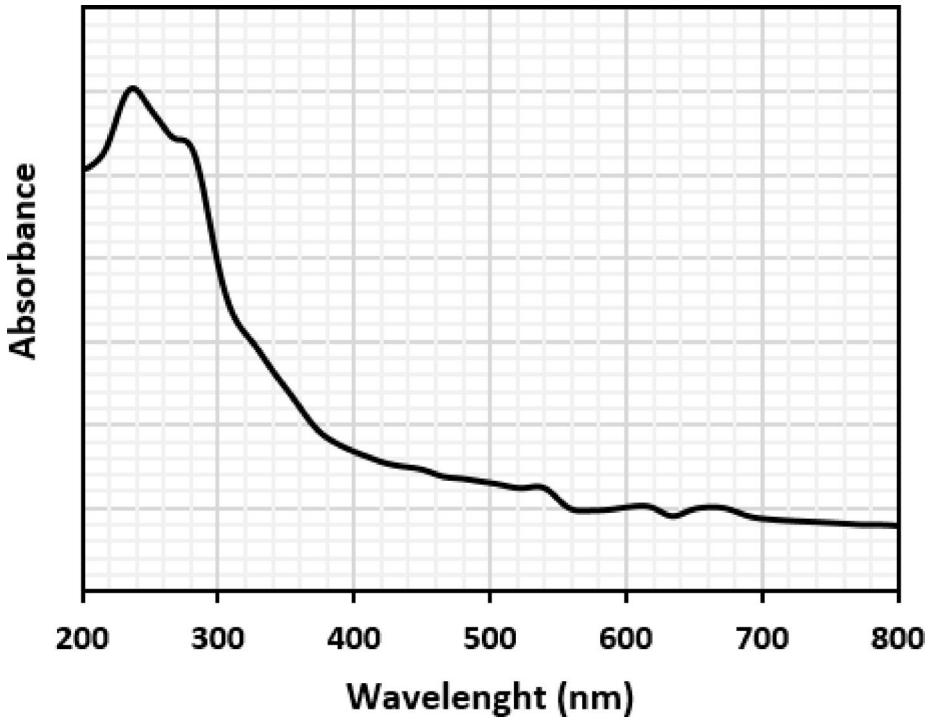

Fig. 6. UV-visible spectrum of the biosynthesized CuO-NPs.

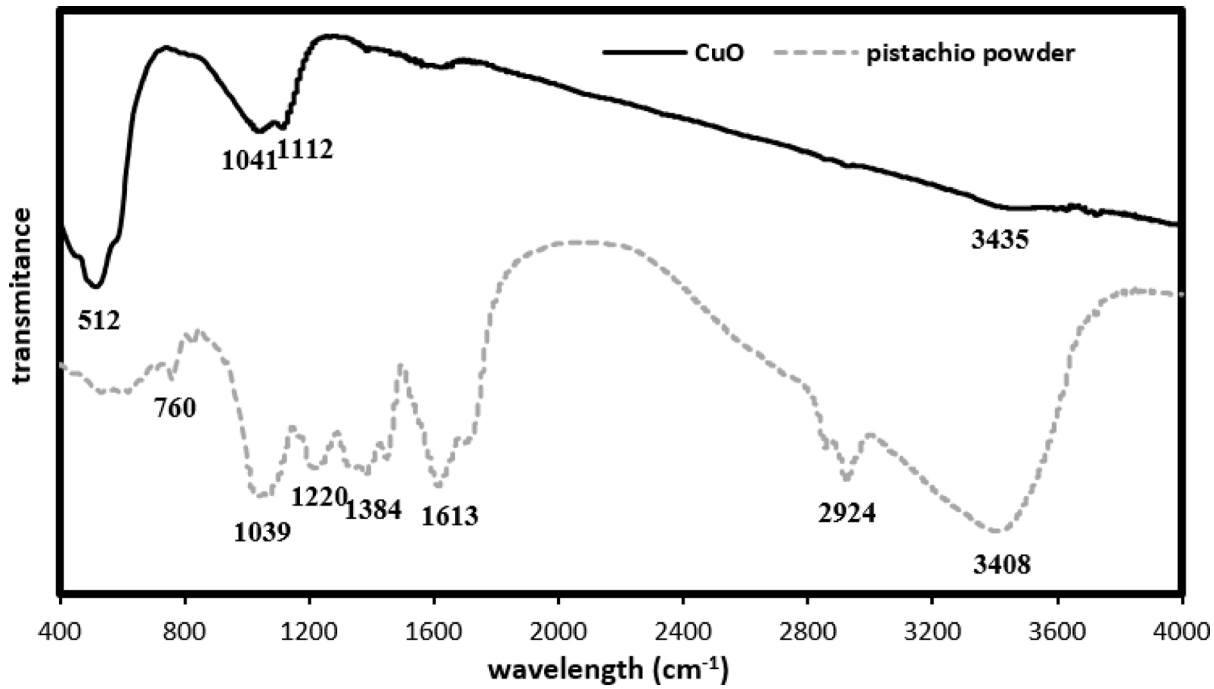

Fig. 7. FTIR spectrum of pistachio hulls and CuO-NPs synthesized in this study.

ultraviolet-visible spectrometer (Photonix Ar 2015), X-ray diffraction (XRD) analysis (PANalytical), filed emission scanning electron microscopy (FESEM- TESCAN MIRA), Fourier Transform Infrared (FTIR) spectroscopy (Nicolet IS10), and dynamic light scattering (DLS) analysis (VEGA III LMU) were applied.

Photocatalytic activity

First, separate solutions of Reactive Blue 21 and Reactive Red 195 with the concentration of 60 mg/L were prepared, and they were briefly named RB21, and RR195. To examine the simultaneous removal of the two

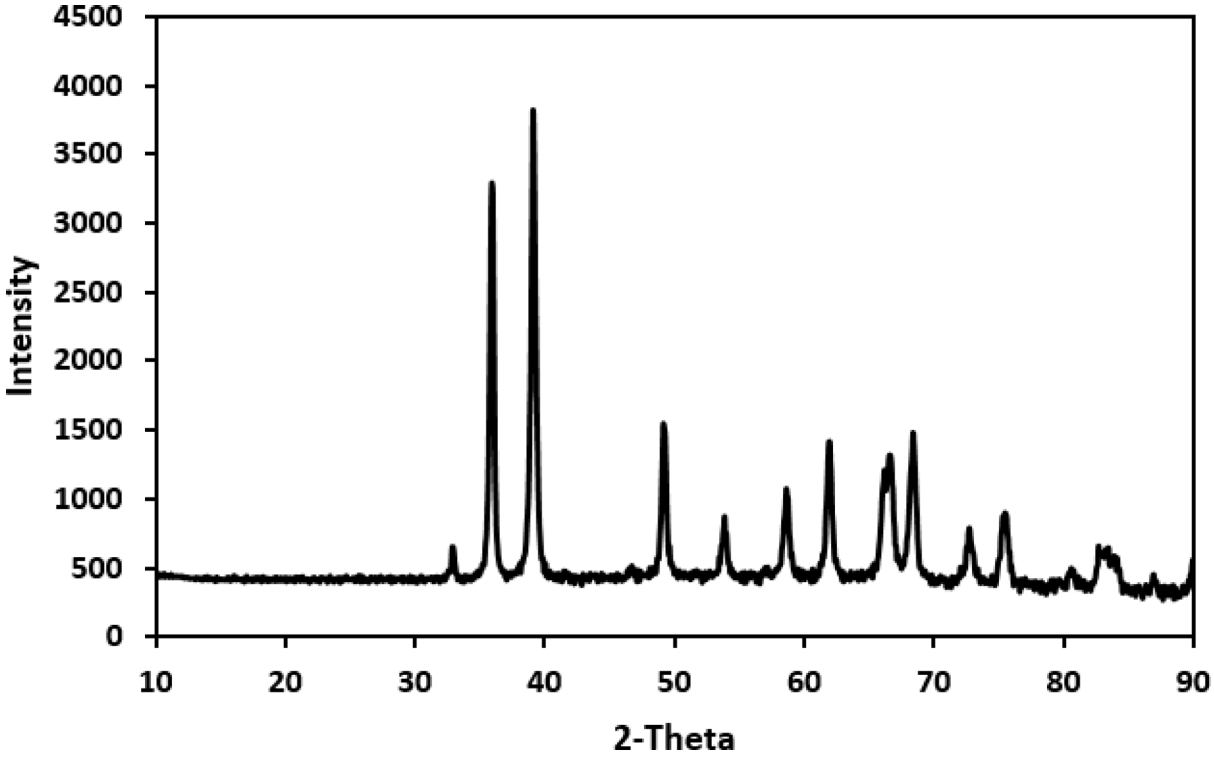

Fig. 8. XRD patterns of the biosynthesized CuO-NPs.

Peak	2θ (°)	d-spacing* (Å)	Miller index	FWHM**	d*** (nm)
1	35.981	2.496	(111)	0.2952	28.3
2	39.142	2.301	(200)	0.2952	28.6
3	49.213	1.851	(202)	0.3542	24.7

Table 2. Crystal lattice parameters of the biosynthesized CuO-NPs. *Calculated by Braggs equation. **Were obtained from the high score plus software. **Crystal size calculated by Scherrer equation.

dyes, 30 mg of each dye was mixed and diluted with distilled water to a final volume of 1000 mL, resulting in a 60 mg/L solution.

0.012 g of biosynthesized CuO-NPs was added to 100 mL of dye solution. The mixture was transferred to a closed wooden chamber with no light exposure and stirred under these dark conditions for sufficient time (about 1 h). The absorbance spectrum of this sample was then recorded and labeled as C_0 (initial concentration). Next, the solution was exposed to UV light emitted from a Philips UV-C lamp (75 watts, 254 nm) while it was being stirred. Air was flowing around the reactor, providing sufficient oxygenation during the photocatalytic degradation process. The reaction temperature was maintained at ambient conditions (40 ± 2 °C) using a water-circulation cooling system.

A small amount of the mixture was sampled every 30 min and was centrifuged at 7000 rpm to separate CuO-NPs, and the absorbance spectrum was recorded. This procedure continued for 180 min, and all data for each dye were collected. The schematic representation of the wooden chamber equipped with UV lamps is shown in (Fig. 5).

For concentration reading by spectrophotometer, the linear calibration curve equation for each dye was required. For this purpose, absorbance spectra were recorded at various known concentrations of the dye solutions, and the peak heights were plotted. Linear regression was applied to obtain the calibration curve equation. Then, the final sample's peak height was substituted into this equation to determine its final concentration.

The obtained final concentration was then substituted into the following formula to calculate the degradation efficiency (η):

$$\eta \ (\%) = \left(\frac{C_0 - C_t}{C_0}\right) \times \ 100 \tag{1}$$

In this equation C_0 is the initial concentration of the dye and C_t is the final concentration after a specified time.

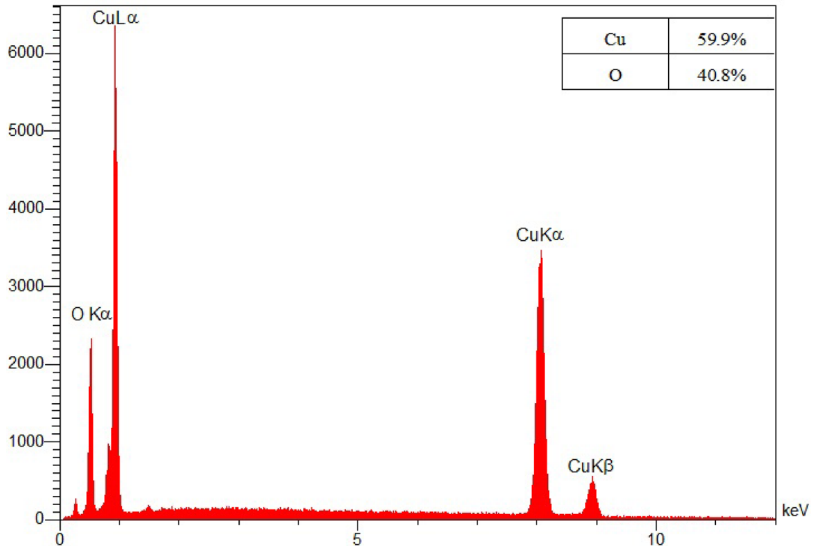

Fig. 9. EDX results for biosynthesized CuO-NPs.

Photocatalytic degradation kinetics

To evaluate the photocatalytic kinetics of dye degradation, the experimental data were fitted to the pseudo-first-order (PFO) model based on dye concentration. The model is expressed as:

$$\ln(\frac{C_0}{C_t}) = K_1 t \tag{2}$$

where C_0 is the initial dye concentration (mg/L), C_t is the dye concentration at time t, and K_1 is the pseudo-first-order rate constant (min^{-1}). By plotting ln (C_0/C_t) versus t, the value of K_1 was obtained from the slope of the linear fit. This approach allows direct comparison of photocatalytic performance with literature reports and provides insight into the rate of dye degradation under UV irradiation.

Results and discussion

Characterization of the biosynthesized CuO-NPs

The UV-visible spectrum of the biosynthesized NPs is shown in (Fig. 6).

The observation of a hump-like absorption peak with a maximum at 240 nm is indeed characteristic and well-documented for the formation of Cupric Oxide (CuO) nanoparticles[43]. During the synthesis of CuO-NPs, the color change from blue to dark brown is a well-established indicator of nanoparticle formation. This transformation corresponds to the excitation of surface plasmon resonance phenomena, which arise from collective oscillations of conduction electrons in response to light[44–46].

FTIR results of the dried pistachio hulls and biosynthesized CuO-NPs are presented in (Fig. 7).

In the spectrum corresponding to CuO nanoparticles, especially between 400 and 600 cm^{-1}, the peak at 512.68 cm^{-1} is the main feature of CuO and is attributed to the Cu–O stretching vibrations. The weak peak at 3435 cm^{-1} is related to the O–H stretching. In the spectrum related to the pistachio hull, the peak at 3407 cm^{-1} corresponds to the O–H stretching (adsorbed water or hydroxyl groups). The peak at 2924 cm^{-1} is assigned to C–H stretching (in methyl or methylene groups). The peak at 1613 cm^{-1} is attributed to H–O–H bending (adsorbed water) or C = O stretching (in carbonyl groups). The peak at 1389 cm^{-1} may be related to C–H bending. The peak at 1220 cm^{-1} corresponds to C–O stretching (in ether or carboxylic acid groups). The peak at 1039 cm^{-1} may also correspond to C–O bonds. The peak at 760 cm^{-1} might be due to out-of-plane C–H vibrations (in aromatic compounds)[6]. Weak FTIR peaks (e.g., ~ 1112 cm^{-1}) suggest trace carbonaceous residues. Such residues may slightly enhance adsorption but do not dominate photocatalysis.

X-ray diffraction (XRD) results of the biosynthesized CuO-NPs are illustrated in Fig. 8.

There are clearly defined peaks at 2Θ=35.80°, 39.14°, 49.21°, which related to monoclinic crystal structure of CuO phase. The results inferred from the mentioned peaks including: spacing between crystal planes (d-spacing), Miller index, full width at half maximum (FWHM), and crystal size (d) of synthesized CuO-NPs are summarized in Table 2.

These results indicate that the nanoparticles are crystalline (fine crystals, about 28 nm), not amorphous. This means the copper atoms are arranged in a regular, repeating pattern. This is crucial for applications where catalytic properties depend on the crystal structure.

EDX (Energy Dispersive X-ray) analysis is an analytical technique used to identify chemical elements in a sample and determine their percentage composition. This method is usually used in conjunction with a scanning electron microscope (SEM). As shown in Fig. 9, the analyzed sample contained copper and oxygen, indicating the successful synthesis of CuO-NPs:

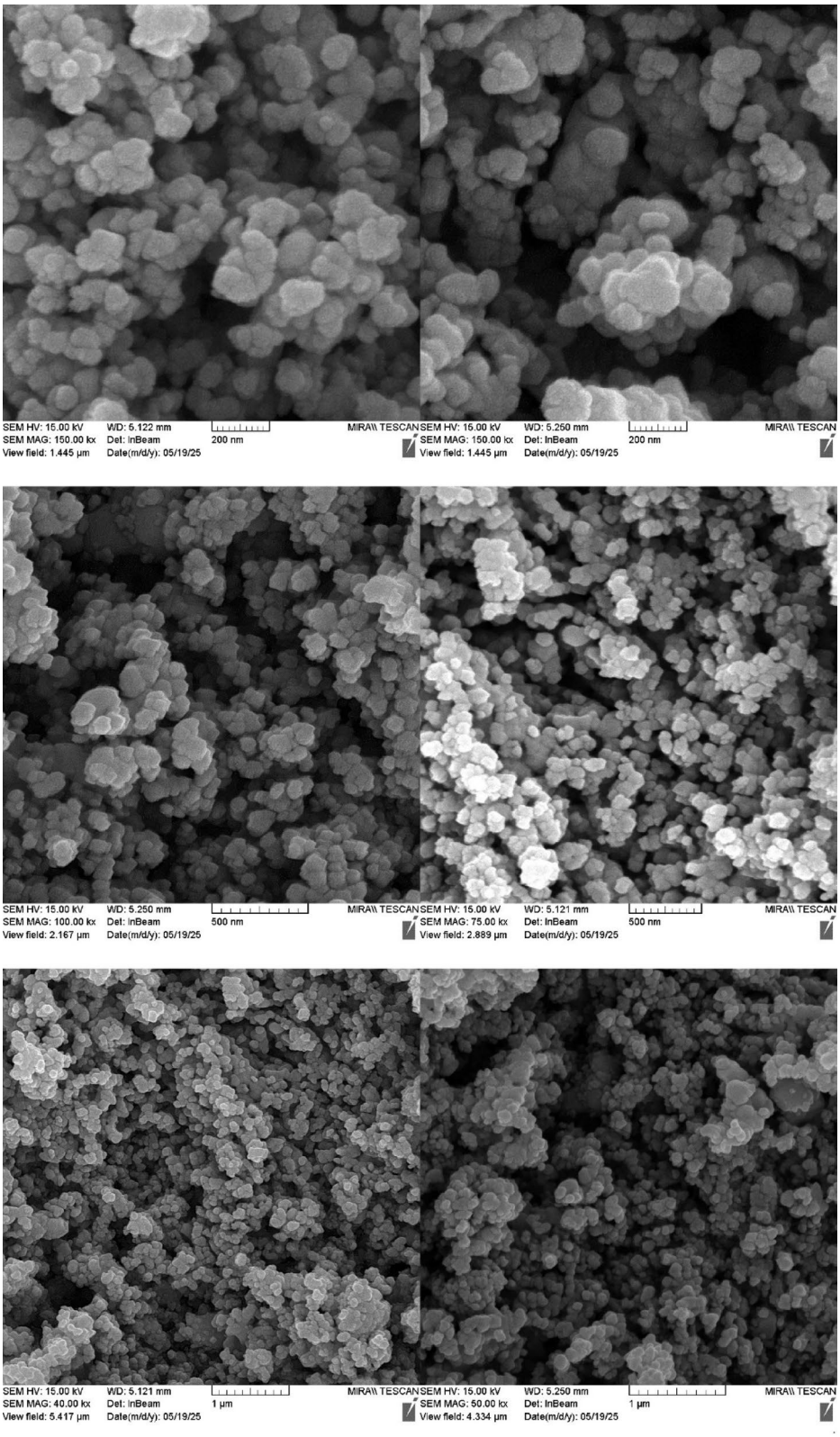

Fig. 10. FESEM images of CuO-NPs synthesized using pistachio hulls extract.

The results of the field emission scanning electron microscopy (FESEM) analysis are seen in Fig. 10. The images were taken at scales of 1 µm, 500 nm, and 200 nm (in order from top to bottom). According to Fig. 8, the size of the spherical particles synthesized using pistachio hull extract is in nano-dimensions below 100 nm.

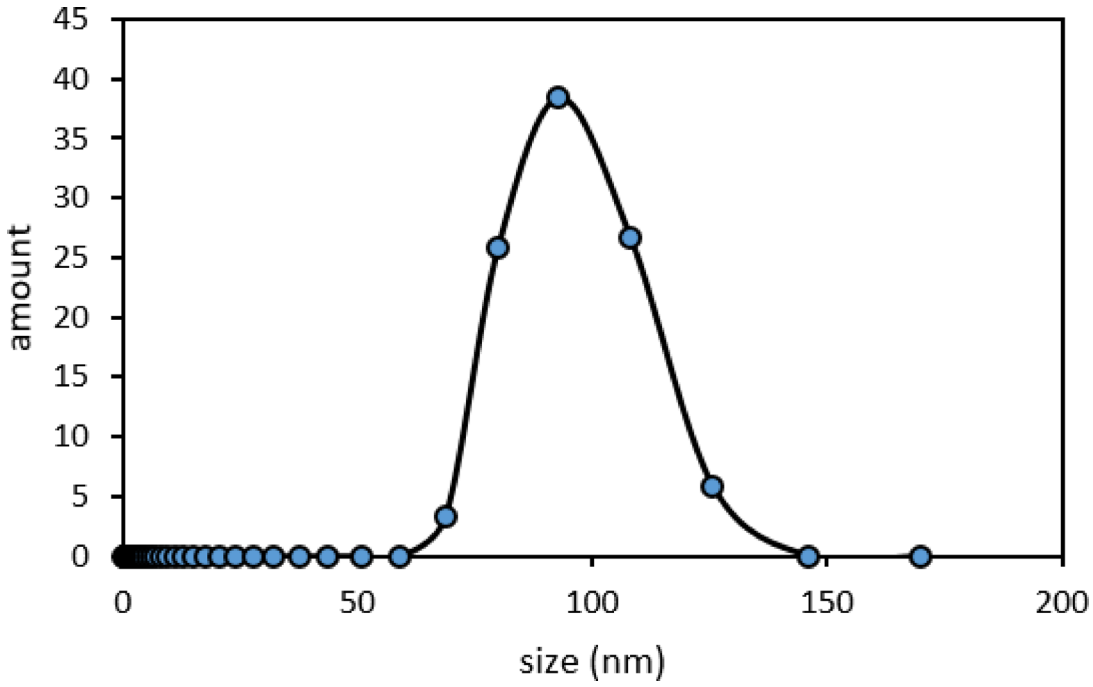

Fig. 11. Particle size distribution of biosynthesized CuO-NPs suspended in water.

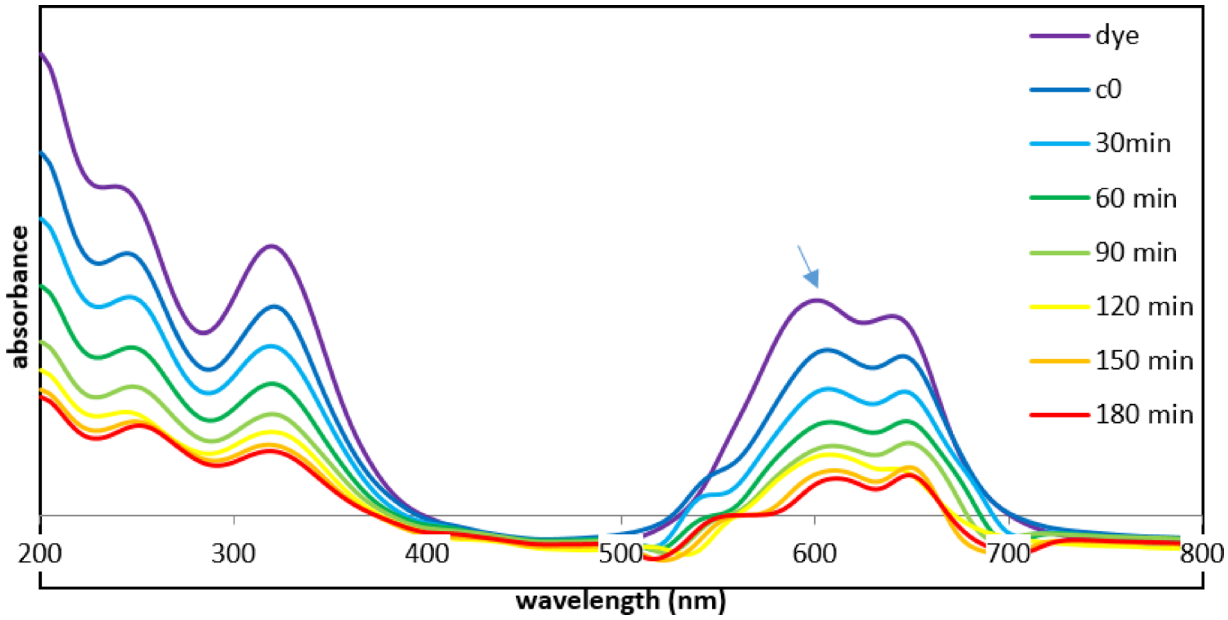

Fig. 12. Absorption spectrum of Reactive Blue 21 solution (60 mg/L) degraded by biosynthesized CuO-NPs with UV irradiation time of 0 to 180 min.

Dynamic Light Scattering (DLS) analysis is a non-destructive physical technique used to determine the particle size distribution of nanoparticles, colloids, or macromolecules suspended in a fluid medium. It relies on measuring random light intensity fluctuations caused by particles undergoing Brownian motion in solution. The results of DLS analysis are shown in Fig. 11. The Gaussian distribution is seen for the suspended CuO particles which have a relatively uniform size spread around an average particle size of about 90 nm, which fits well within nanoscale measurement contexts. The measured size difference between XRD and FESEM/DLS is attributed to polycrystalline aggregation of primary crystallites during synthesis/drying, a common phenomenon in green-synthesized NPs.

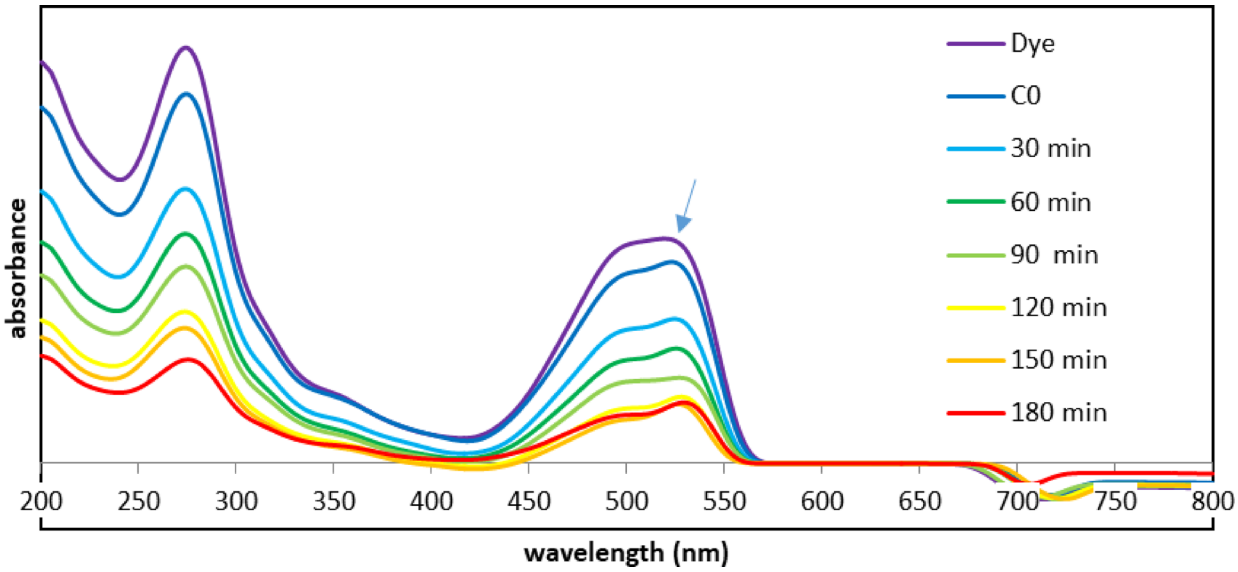

Fig. 13. Absorption spectrum of Reactive Red 195 solution (60 mg/L) degraded by biosynthesized CuO-NPs with UV irradiation time of 0 to 180 min.

Photocatalytic degradation

The effect of irradiation time on the degradation process was assessed by analyzing changes in the UV-vis absorption spectra. Figure 12 shows a substantial reduction in the absorbance intensity at 615 nm (primary peak for Reactive Blue 21 in visible region) corresponding to a degradation efficiency of 83%. These results confirm the exceptional photocatalytic performance of biosynthesized CuO-NPs in decomposing the organic dye.

Absorption spectrum of Reactive Red 195 solution degraded by biosynthesized CuO-NPs with UV irradiation time of 0 to 180 min is presented in Fig. 13. It is clear that the absorbance peak intensity of Reactive Red 195 dye at 530 nm released strangely with the increase of irradiation time and degradation rate reached 75%.

The efficiency degradation dye (Reactive Blue 21 and Reactive Red 195) over irradiation time is illustrated in Fig. 14a. It can be concluded that biosynthesized CuO-NPs catalyst has higher photocatalytic activity in the degradation of Reactive Blue 21 than Reactive Red 195 in all of the irradiation time.

The results of degradation efficiency in the mixed solution dye are shown in Fig. 14b. A comparative analysis of the degradation efficiency revealed a fairly significant decrease in the removal rate of both Reactive Blue 21 and Reactive Red 195 within the binary mixture, as opposed to their individual degradation profiles. Specifically, after 180 min of irradiation, the degradation efficiency for Reactive Blue 21 was 69% and for Reactive Red 195 was 60% in the mixture, values relatively lower than those achieved when the dyes were processed separately. This observed suppression in efficiency is attributed to competitive effects between the two dye molecules for active sites on the photocatalyst surface and for the generated reactive oxidative species (e.g., •OH, O_2•$^-$).

Absorption spectrum results of a binary dye system (Reactive Blue 21 / Reactive Red 195) are presented in Fig. 15. This result exhibits somewhat distinct and resolved absorption peaks in the visible region, with maxima at approximately 615 nm and 530 nm, respectively. This relative spectral separation allows for the independent monitoring of each dye's degradation kinetics by tracking the decrease in absorbance at their characteristic λ_{max} values over the course of the photocatalytic reaction. On the other hand, the absorption bands of the two dyes overlap greatly in the ultraviolet region and no information can be deduced in this range.

Photocatalytic degradation kinetics

The graph of $Ln(C_0/C_t)$ was plotted against time (Fig. 16) and the value of K_1 from Eq. 2, which was equal to the slope of the line, was obtained from curve fitting. The value of the coefficient K_1 in different cases is reported in Table 3.

The results indicate that the degradation of both dyes follows pseudo-first-order kinetics with good linearity. Moreover, the rate constants obtained for the individual dye solutions were higher than those for the mixed solution, suggesting competitive adsorption and reduced availability of active sites in the presence of both dyes simultaneously. This kinetic modeling not only confirms the reproducibility of the photocatalytic process but also enables direct comparison with existing literature, highlighting the efficiency of pistachio hull–derived CuO nanoparticles in dye degradation. Both dyes are anionic; RB21 likely has stronger adsorption than RR195, explaining its higher K1. According to non-overlapping visible peaks, photon competition is minimal. Radical scavenging is possible, but adsorption competition is the dominant factor, as degradation drops proportionally for both dyes.

Reaction mechanism

A schematic description of the photocatalytic mechanism of biosynthesized CuO-NPs are shown in Fig. 17. When CuO-NPs are irradiated with UV light energy equal to or greater than their band gap (~ 3.8 eV), electrons (e^-) in

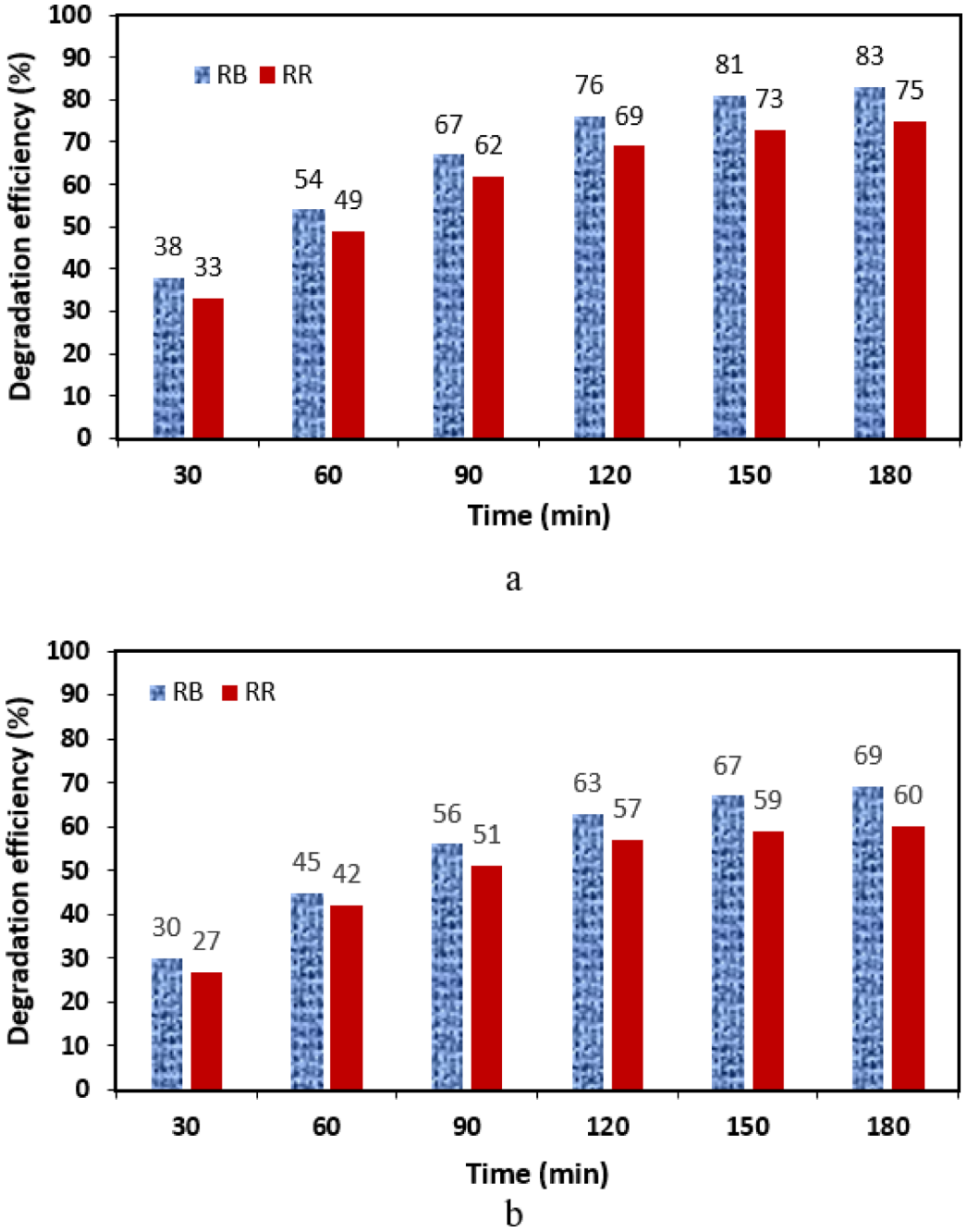

Fig. 14. The degradation efficiency of dye over irradiation time (**a**) Reactive Blue 21 and Reactive Red 195 (separate solutions), and (**b**) mixed dye.

the valence band (VB) are excited to the conduction band (CB), leaving behind positive holes (h^+) in the VB. The excited electrons and holes act as reactive species. Electrons in the CB can reduce oxygen molecules adsorbed on the surface to form superoxide radicals ($.O_2^-$), while holes in the VB can oxidize water or hydroxyl ions to form hydroxyl radicals (.OH). These radicals attack the dye's complex azo structure, leading to the cleavage of azo bonds (-N = N-), and breakdown of aromatic rings and sulfonic groups. Typical degradation products include: smaller aromatic amines, carboxylic acids, sulfates and sulfites from sulfonic groups, eventually mineralized products such as CO_2, H_2O, NH^{4+}, and NO^{3-} upon complete degradation. As degradation proceeds, the CuO surface sites are regenerated for ongoing photocatalytic cycles under continuous light exposure.

Conclusion

This study successfully demonstrated the eco-friendly synthesis of copper oxide nanoparticles (CuO-NPs) using pistachio hull extract and their effective application in degrading persistent textile dyes. CuO-NPs were biosynthesized using an aqueous extract of pistachio hulls, which acted as both reducing and stabilizing agents.

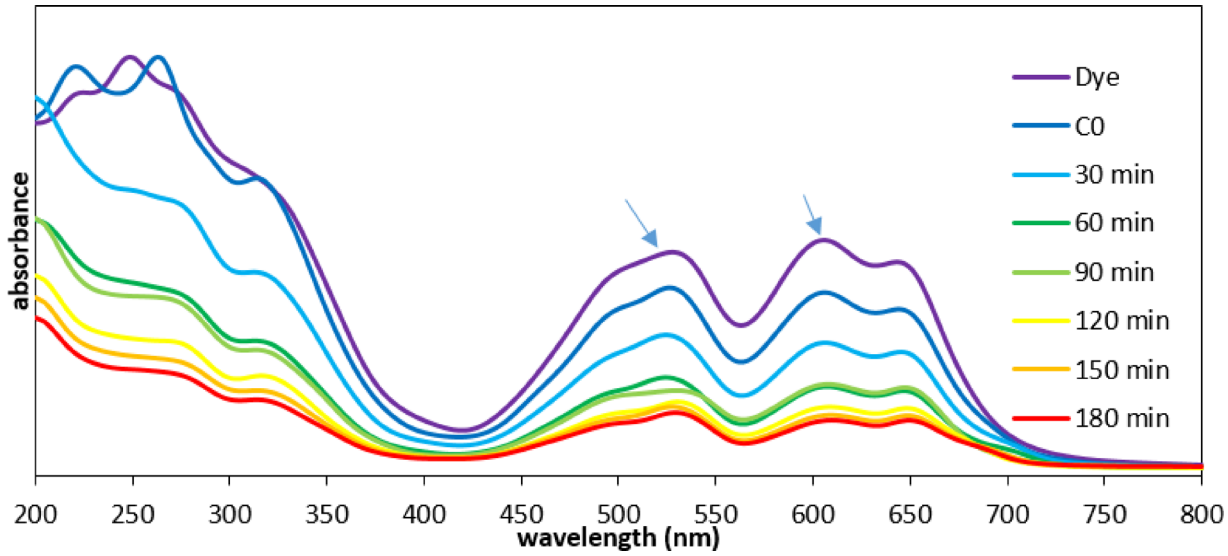

Fig. 15. Absorption spectrum of mixed dye solution (Reactive Blue 21 / Reactive Red 195) (60 mg/L) degraded by biosynthesized CuO-NPs with UV irradiation time of 0 to 180 min.

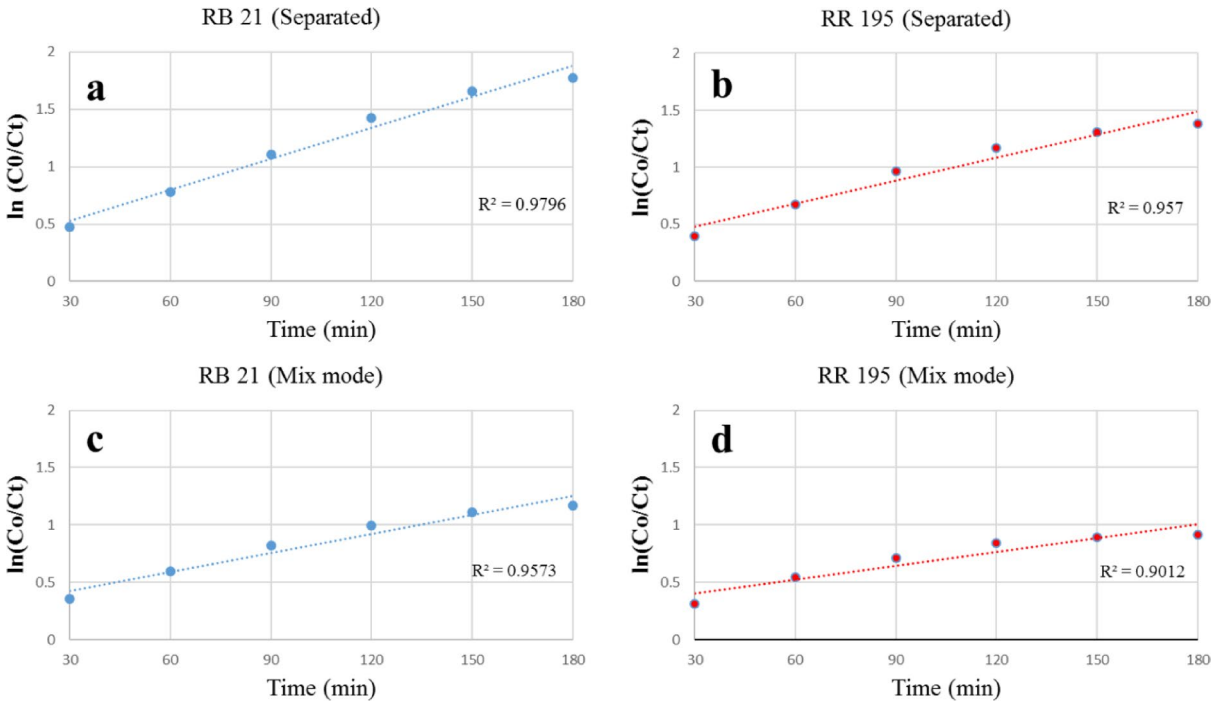

Fig. 16. Graphs of changes in ($\ln(C_0/C_t)$) over time for (**a**) RB21 in separated solution, (**b**) RR195 in separated solution, (**c**) RB21 in mix solution and (**d**) RR195 in mix solution.

Comprehensive characterization (XRD, SEM, FT-IR, DLS, UV-Vis) confirmed the formation of homogeneous, spherical, and crystalline nanoparticles with an average size of 90 nm. The FTIR spectrum of pistachio hull extract confirms the presence of hydroxyl and carbonyl groups, which are consistent with phenolic and flavonoid compounds. These functional groups not only participate in the reduction of Cu^{2+} ions but also remain adsorbed on the nanoparticle surface, providing steric hindrance against agglomeration. The resulting spherical morphology and narrow size distribution observed in FESEM images can thus be directly linked to the stabilizing role of these phytochemicals. This chemical justification highlights why pistachio hull extract is particularly effective compared to other plant-based reducing agents. The photocatalytic activity of these green-synthesized nanoparticles was evaluated against two reactive dyes, Reactive Blue 21 and Reactive Red 195, under UV light. The biosynthesized CuO-NPs exhibited high efficiency, achieving 83% degradation of RB 21 and 75%

Dye	K_1
RB21 (separated solution)	0.00899
RR195 (separated solution)	0.00773
RB21 (Mix)	0.00647
RR195 (MIX)	0.00442

Table 3. Calculated K1 in different situation for RB21 and RR185.

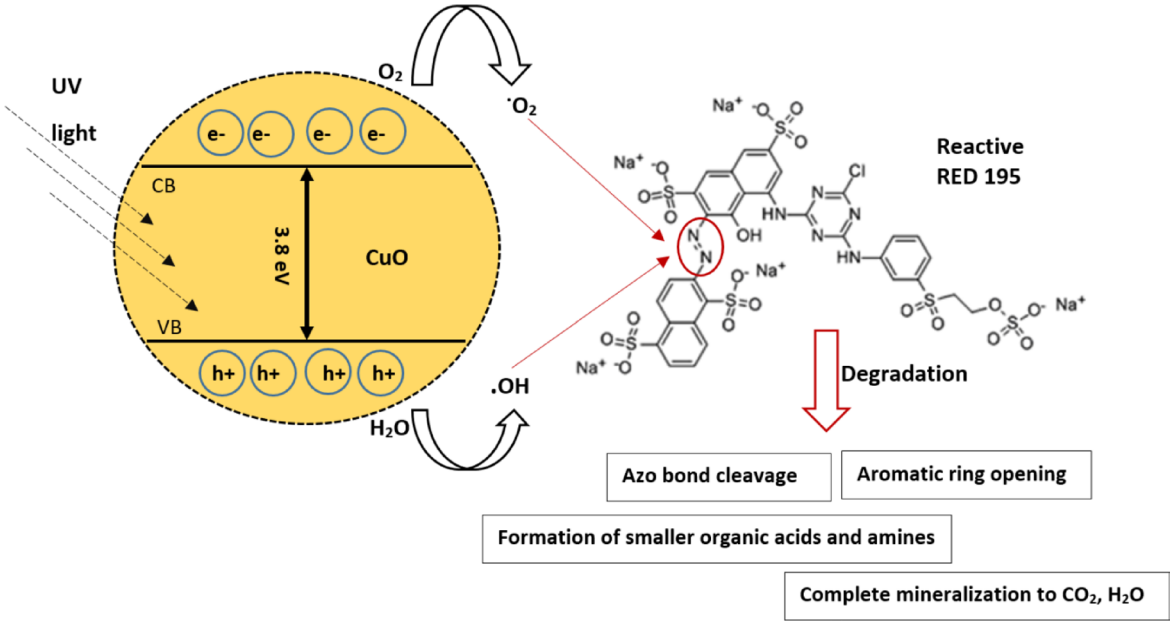

Fig. 17. Schematic description of the photocatalytic mechanism of biosynthesized CuO-NPs with Reactive Red 195.

degradation of RR 195 within 180 min. The study was extended to a mixture of Reactive Blue 21 and Reactive Red 195 to simulate more complex, real-world wastewater. UV-Visible spectroscopy was used to monitor the degradation, but a key analytical challenge was noted. The dyes' absorption peaks are somewhat distinct in the visible region, allowing for individual quantification. However, their absorption bands overlap significantly in the ultraviolet region, making that spectral range unusable for analysis. The research successfully demonstrates that pistachio hull extract can be used to synthesize effective CuO-NPs. These biosynthesized CuO-NPs are potent photocatalysts for degrading textile dyes, both individually and in a mixture, although monitoring degradation in mixtures requires careful analysis of non-overlapping spectral regions.

One of the aims of this research, to reuse pistachio hulls as agricultural waste from the Rafsanjan region of Iran, is well justified by the scale and potential of pistachio byproducts in that area. For every ton of fresh pistachio nuts, roughly 300–400 kg of wet hulls are generated as by-products during processing. Given Rafsanjan's large-scale operations, this translates to tens of thousands of tons of pistachio hulls annually, forming a significant and renewable stream of agricultural waste.

Data availability

Data will be made available on reasonable request.The datasets generated and/or analyzed during the current study are not publicly available but are available from the corresponding author on reasonable request.

Received: 5 November 2025; Accepted: 16 February 2026
Published online: 24 February 2026

References

1. Islam, T., Repon, M. R., Islam, T., Sarwar, Z. & Rahman, M. M. Impact of textile dyes on health and ecosystem: a review of structure, causes, and potential solutions. *Environ. Sci. Pollut. Res.* **30** (4), 9207–9242 (2023).
2. Teo, S. H. et al. Sustainable toxic dyes removal with advanced materials for clean water production: A comprehensive review. *J. Clean. Prod.* **332**, 130039 (2022).
3. Tripathi, M. et al. Recent strategies for the remediation of textile dyes from wastewater: a systematic review. *Toxics* **11** (11), 940 (2023).

4. Khan, S., Noor, T., Iqbal, N. & Yaqoob, L. Photocatalytic dye degradation from textile wastewater: a review. *ACS omega*. **9** (20), 21751–21767 (2024).
5. Hunger, K. *Industrial dyes: chemistry, properties, applications* (Wiley, 2007).
6. Vanaamudan, A. & Chavada, B. Adsorption of reactive blue 21 and reactive red 141 from aqueous solutions onto hydrotalcite. *J. Environ. Chem. Eng.* **4** (3), 2617–2627 (2016).
7. Alaqarbeh, M. Adsorption phenomena: definition, mechanisms, and adsorption types: short review. *RHAZES: Green. Appl. Chem.* **13**, 43–51 (2021).
8. Saeed, M., Muneer, M., Haq, A. U. & Akram, N. Photocatalysis: an effective tool for photodegradation of dyes—a review. *Environ. Sci. Pollut. Res.* **29** (1), 293–311 (2022).
9. Yue, Y. et al. Synergistic adsorption and photocatalysis study of TiO_2 and activated carbon composite. *Heliyon* **10** (10), e30817 (2024).
10. Rodrigues, J., Hatami, T., Rosa, J. M. & Tambourgi, E. B. Photocatalytic degradation of Reactive Blue 21 dye using ZnO nanoparticles: experiment, modelling, and sensitivity analysis. *Environ. Technol.* **42** (23), 3675–3687 (2021).
11. El-Bindary, A., Ismail, A. & Eladl, E. Photocatalytic degradation of reactive blue 21 using Ag doped ZnO nanoparticles. *J. Mater. Environ. Sci.* **10** (12), 1258–1271 (2019).
12. Sarkar, S., Mohanty, S., Moulick, S., Adak, A. & Maji, S. K. Adsorption/Photodegradation of reactive blue (Cl No. 21) from aqueous media by hydrothermally synthesized titanate nanotube (TNT). In *AIP Conference Proceedings* (Vol. 2740, No. 1, p. 060007). (AIP Publishing LLC, 2023).
13. Jouali, A. et al. Photo-catalytic degradation of methylene blue and reactive blue 21 dyes in dynamic mode using TiO2 particles immobilized on cellulosic fibers. *J. Photochem. Photobiol., A*. **383**, 112013 (2019).
14. Atrak, K., Ramazani, A. & Taghavi Fardood, S. Green synthesis of Zn0. 5Ni0. 5AlFeO4 magnetic nanoparticles and investigation of their photocatalytic activity for degradation of reactive blue 21 dye. *Environ. Technol.* **41** (21), 2760–2770 (2020).
15. Feliczak-Guzik, A. Nanomaterials as photocatalysts—synthesis and their potential applications. *Materials* **16** (1), 193 (2022).
16. Abdelbasir, S. M., McCourt, K. M., Lee, C. M. & Vanegas, D. C. Waste-derived nanoparticles: synthesis approaches, environmental applications, and sustainability considerations. *Front. Chem.* **8**, 782 (2020).
17. Radulescu, D. M. et al. Green synthesis of metal and metal oxide nanoparticles: a review of the principles and biomedical applications. *Int. J. Mol. Sci.* **24** (20), 15397 (2023).
18. Hussain, I., Singh, N. B., Singh, A., Singh, H. & Singh, S. C. Green synthesis of nanoparticles and its potential application. *Biotechnol. Lett.* **38** (4), 545–560 (2016).
19. Jadoun, S., Arif, R., Jangid, N. K. & Meena, R. K. Green synthesis of nanoparticles using plant extracts: A review. *Environ. Chem. Lett.* **19** (1), 355–374 (2021).
20. Alabrahim, O. A., Abdeldayem, A. M. & Azzazy, H. M. Green synthesis of metallic nanoparticles using Pistacia species: improved stability and biological activities. *Nanoscale Adv.* (2025).
21. Kalaiyan, G. et al. Green synthesis of copper oxide nanoparticles using Euphorbia heterophylla leaf extract for deactivation of pathogenic bacteria and photocatalytic degradation of industrial dyes. *Results Eng.* **26**, 104797 (2025).
22. Chandraker, S. K. et al. Green synthesis of copper nanoparticles using leaf extract of Ageratum houstonianum Mill. and study of their photocatalytic and antibacterial activities. *Nano Express*. **1** (1), 010033 (2020).
23. Ramzan, M. et al. Green synthesis of copper oxide nanoparticles using Cedrus deodara aqueous extract for antibacterial activity. *Mater. Today: Proc.* **36**, 576–581 (2021).
24. Andualem, W. W. et al. Synthesis of copper oxide nanoparticles using plant leaf extract of Catha edulis and its antibacterial activity. *J. Nanatechnol.* **2020** (1), 2932434 (2020).
25. Sathiyavimal, S. et al. Green synthesis of copper oxide nanoparticles using Abutilon indicum leaves extract and their evaluation of antibacterial, anticancer in human A549 lung and MDA-MB-231 breast cancer cells. *Food Chem. Toxicol.* **168**, 113330 (2022).
26. Yugandhar, P. et al. Bioinspired green synthesis of copper oxide nanoparticles from Syzygium alternifolium (Wt.) Walp: characterization and evaluation of its synergistic antimicrobial and anticancer activity. *Appl. Nanosci.* **7**, 417–427 (2017).
27. Vasantharaj, S. et al. Antibacterial activity and photocatalytic dye degradation of copper oxide nanoparticles (CuONPs) using Justicia gendarussa. *Appl. Nanosci.* **13** (3), 2295–2302 (2023).
28. Singh, J. et al. Biogenic synthesis of copper oxide nanoparticles using plant extract and its prodigious potential for photocatalytic degradation of dyes. *Environ. Res.* **177**, 108569 (2019).
29. Rafique, M. et al. Eco-friendly green and biosynthesis of copper oxide nanoparticles using Citrofortunella microcarpa leaves extract for efficient photocatalytic degradation of Rhodamin B dye form textile wastewater. *Optik* **208**, 164053 (2020).
30. Eid, A. M. et al. Plant-based copper oxide nanoparticles; biosynthesis, characterization, antibacterial activity, tanning wastewater treatment, and heavy metals sorption. *Catalysts* **13** (2), 348 (2023).
31. Mirhadi, H., Momeni, A. & Meshkatalsadat, M. H. Biogenic Synthesis of Copper Oxide Nanoparticles Using Falcaria vulgaris L. Leaf Extract and Assessment of Its Antibacterial Activity against Salmonella Paratyphi-A. *Nano Biomed. Eng.* **16** (3), 473–483 (2024).
32. Komara, J., Karumuri, J. P. & Naik, B. S. S. Green synthesis of copper oxide nanoparticles using solanum melongena seeds extract and its applications in degradation of Rose Bengal dye, antibacterial, catalytic reduction and antioxidant activity. *Hybrid. Adv.* **7**, 100304 (2024).
33. Eskandari, P. et al. Investigation of antimicrobial properties of green synthesized CuO nanostuctures using Berberis integerrima aqueous extract on infected surgical wound caused by Staphylococcus aureus. **16** (3), pp. 99–111. (2023).
34. Chaikali, C. et al. Green Synthesis and Comparative Analysis of Silver, Copper Oxide, and Bimetallic Ag/CuO Nanoparticles Using Cistus creticus L. Extract: Physicochemical Properties, Stability, and Antioxidant Potential. *Int. J. Mol. Sci.* **26** (6), 2518 (2025).
35. Haseki, S. et al. Influence of synthesis method on physiochemical properties and antibacterial activity of green synthesized CuO nanoparticles from Laurus nobilis L. leaf extracts. *Plant. Nano Biology*. **11**, 100128 (2025).
36. Anwaar, S. et al. Biogenic synthesis of copper oxide nanoparticles using Eucalyptus globulus Leaf Extract and its impact on germination and Phytochemical composition of Lactuca sativa. *Sci. Rep.* **14** (1), 1–5 (2024).
37. Veisi, H. et al. Biosynthesis of CuO nanoparticles using aqueous extract of herbal tea (Stachys Lavandulifolia) flowers and evaluation of its catalytic activity. *Sci. Rep.* **11** (1), 1983–p (2021).
38. Muthuvel, A., Jothibas, M. & Manoharan, C. Synthesis of copper oxide nanoparticles by chemical and biogenic methods: photocatalytic degradation and in vitro antioxidant activity. *Nanatechnol. Environ. Eng.* (2), 14. (2020).
39. Vaidehi, D., Bhuvaneshwari, V., Bharathi, D. & Sheetal, B. P. Antibacterial and photocatalytic activity of copper oxide nanoparticles synthesized using Solanum lycopersicum leaf extract. *Mater. Res. Express*. **5** (8), 085403 (2018).
40. Shashanka, R. Investigation of optical and thermal properties of CuO and ZnO nanoparticles prepared by Crocus Sativus (Saffron) flower extract. *J. Iran. Chem. Soc.* **18** (2), 415–427 (2021).
41. Surendhiran, S. et al. Rapid green synthesis of CuO nanoparticles and evaluation of its photocatalytic and electrochemical corrosion inhibition performance. *Mater. Today: Proc.***47**, 1011-6. (2021).
42. Taghizadeh, A. & Rad-Moghadam, K. Green fabrication of Cu/pistachio shell nanocomposite using Pistacia Vera L. hull: An efficient catalyst for expedient reduction of 4-nitrophenol and organic dyes. *J. Clean. Prod.* **198**, 1105–1119 (2018).
43. Manjunatha, K. et al. Antimicrobial and nonlinear optical studies of copper oxide nanoparticles. *J. Electron. Mater.* **50**, 3415–3421 (2021).

44. Mobarak, M. B., Hossain, M. S., Chowdhury, F. & Ahmed, S. Synthesis and characterization of CuO nanoparticles utilizing waste fish scale and exploitation of XRD peak profile analysis for approximating the structural parameters. *Arab. J. Chem.* **15** (10), 104117 (2022).
45. Kamble, S. P. & Mote, V. D. Structural, optical and magnetic properties of Co doped CuO nano-particles by sol-gel auto combustion technique. *Solid State Sci.* **95**, 105936 (2019).
46. Maheo, A. R., Vithiya, B. S., Prasad, T. A., Tamizhdurai, P. & Mangesh, V. L. Biosynthesis, characterization, biological and photo catalytic investigations of Elsholtzia blanda and chitosan mediated copper oxide nanoparticles. *Arab. J. Chem.* **15** (3), 103661 (2022).

Author contributions

Seyed Mohammad Sadegh Hosseini: Conceptualization, Methodology, Writing- Original draft preparation. Mohammad Ali Maghool: Experimental Investigation, Data curation. Hadis Eghbali: Conceptualization, Writing-Reviewing and Editing,

Declarations

Competing interests

The authors declare no competing interests.

Additional information

Correspondence and requests for materials should be addressed to S.M.S.H.

Reprints and permissions information is available at www.nature.com/reprints.

Publisher's note Springer Nature remains neutral with regard to jurisdictional claims in published maps and institutional affiliations.

Open Access This article is licensed under a Creative Commons Attribution-NonCommercial-NoDerivatives 4.0 International License, which permits any non-commercial use, sharing, distribution and reproduction in any medium or format, as long as you give appropriate credit to the original author(s) and the source, provide a link to the Creative Commons licence, and indicate if you modified the licensed material. You do not have permission under this licence to share adapted material derived from this article or parts of it. The images or other third party material in this article are included in the article's Creative Commons licence, unless indicated otherwise in a credit line to the material. If material is not included in the article's Creative Commons licence and your intended use is not permitted by statutory regulation or exceeds the permitted use, you will need to obtain permission directly from the copyright holder. To view a copy of this licence, visit http://creativecommons.org/licenses/by-nc-nd/4.0/.

© The Author(s) 2026